Eur. Phys. J. B **45**, 137–146 (2005)
DOI: 10.1140/epjb/e2005-00172-9

THE EUROPEAN PHYSICAL JOURNAL B

A study of the induced magnetism in the Au spacer layer of Co/Au/CoO exchange-bias trilayers and related systems

M. Gierlings[1], M.J. Prandolini[1,2,a], M. Gruyters[3], T. Funk[4], D. Riegel[1], and W.D. Brewer[2]

[1] Hahn-Meitner Institut Berlin, 14109 Berlin, Glienicker Strasse 100, Germany
[2] Institut für Experimentalphysik, Freie Universität Berlin, Arnimallee 14, 14195 Berlin-Dahlem, Germany
[3] Humboldt-Universität zu Berlin, Institut für Physik, 12489 Berlin, Germany
[4] UCSF, San Francisco CA, USA

Received 17 November 2004
Published online 16 June 2005 –

Abstract. We report the first observation of the effects of exchange bias on the nuclear spin polarization and induced magnetic moments at a magnetic/non-magnetic interface, applying **l**ow **t**emperature **n**uclear **o**rientation (LTNO) to Co/Au(x)/CoO trilayer systems. This technique allows us to determine simultaneously the average alignment of the nuclear moments for the two radioactive probe isotopes ^{198}Au and ^{60}Co with respect to an external magnetic field axis. The total average Au γ-ray anisotropy measured was found (i) to decrease with increasing Au thickness, indicating that large hyperfine fields are restricted to the interfacial Au layers and (ii) to be canted away from the applied field axis even when the Co layers are magnetically saturated. This canting was found to originate at the CoO/Au interface as could be shown from comparative measurements on CoO/Au/CoO trilayers containing two AFM CoO/Au interfaces and on a Co/Au/Co trilayer with two FM Co/Au interfaces. In the case of CoO/Au/CoO, the observed canting was found to be dependent on the Au layer thickness.

PACS. 75.70.-i Magnetic films and multilayers – 75.70.Cn Interfacial magnetic properties – 31.30.Gs Hyperfine interactions

1 Introduction

The introduction of a non-magnetic spacer layer into a simple magnetic system allows for the possibility of engineering its magnetic properties to be drastically different from bulk characteristics. The first such systems investigated were ferromagnetic (FM)/spacer/FM structures. By varying the spacer composition and/or thickness, it was discovered that the coupling between FM layers could be changed from ferromagnetic to antiferromagnetic (AFM) [1].

Recently, a classical exchange bias (EB) system, consisting of a simple FM/AFM bilayer, was also modified to include a spacer (FM/spacer/AFM) [2]. The EB effect occurs in many ferromagnetic materials when they are coupled to an AFM [3,4] surface, and it manifests itself in hysteresis loops whose centers are shifted away from the zero-field axis. One possibility to induce the EB effect is by field cooling a FM/AFM bilayer below the Néel temperature of the AFM. In many systems, the strength of the induced EB and the magnetic coercivity then increase with decreasing temperature.

Originally, EB was thought to be exclusively an interface effect; however, it was then experimentally shown that magnetic coupling can also occur across a non-magnetic 'spacer', e.g. Cu, Ag or Au, in FM/spacer/AFM systems [2,5–7]. In all cases where the EB strength has been investigated as a function of the spacer thickness, the induced EB and the coercivity were found to decrease with increasing spacer thickness. Above a critical spacer thickness, which has proved to be material dependent, the EB effect vanishes. Nevertheless, it has not yet been established whether interlayer exchange coupling in FM/spacer/AFM systems is a general phenomenon, and there remains some controversy as to whether the EB effect is transferred through 'pinholes' in the spacer or whether it is in fact a long-range coupling persisting through the non-magnetic spacer [8]. However, it is clear that the coupling in EB systems is strongly influenced by the interactions at the FM/AFM interface. The introduction of a non-magnetic spacer such as Cu, Ag or Au between the FM and AFM layers modifies this interface coupling. Therefore it is of great interest to obtain information on the spin directions in the vicinity of the interface, especially in the non-magnetic spacer, and to study how induced magnetic moments are formed in or transferred across a spacer layer.

[a] e-mail: prandoli@physik.fu-berlin.de

In order to understand systematically the complicated interactions in a FM/spacer/AFM EB system, we have performed comparative measurements on related trilayer systems containing two interfaces of the same type: (i) a FM/spacer/FM trilayer with two FM/spacer interfaces and (ii) AFM/spacer/AFM trilayers with two AFM/spacer interfaces. We begin by investigating the AFM/spacer/AFM trilayers. This type of magnetic system containing intrinsic AFM materials has rarely been experimentally addressed. For most AFM materials with Néel temperatures near room temperature, the magnetic anisotropy field is prohibitively high (well over 10 T) [9]. Furthermore, most experimental techniques are sensitive only to macroscopic detection of the magnetization, and thus will have difficulties investigating these systems without a FM "sensor" layer.

The low-temperature nuclear orientation (LTNO) technique detects the average magnitude and alignment of the nuclear spins, ($\langle I_z^2 \rangle$), of radioactive probe nuclei [10]. In the case of the neutron-activated Co/Au/CoO EB systems and related trilayer samples studied here, these probe nuclei are ^{60}Co and ^{198}Au, which result from neutron capture by the naturally-occurring Co and Au isotopes. Generally, for the majority of radioactive probes cooled to mK temperatures, a local magnetic hyperfine field of over ~ 3 T is required to obtain observable nuclear alignment by this technique. Previous theoretical [11] and experimental [12] hyperfine interactions studies on metallic FM/noble-metal thin film systems have shown that large induced spin polarizations at the site of the probe atoms (hyperfine fields ≥ 3 T) in a thin non-magnetic spacer are to be expected exclusively in the atomic layer adjacent to the interface with a magnetic material. The magnetic hyperfine fields of the non-magnetic spacer atoms in the second and third layers away from the magnetic interface generally have magnetic moments and hyperfine fields 10 times smaller than the atoms at the interface. In particular, this has been demonstrated experimentally using perturbed angular correlations (PAC) studies on Fe/Ag bilayers with ^{111}In probes [13]; on Fe/Ag multilayers using LTNO [12]; as well as with Mössbauer spectroscopy performed on Au/Ni and Au/Fe multilayers [14] and with XMCD on Ni/Pt multilayers [15].

However, AFM/spacer interfaces containing an intrinsic AFM material, such as CoO, have thus far not been been investigated in this way. A secondary aim of this work is therefore the extension of this picture to the Au hyperfine fields at the more complex AFM CoO/Au interface, i.e. to test whether the observed LTNO signal is found to decrease as the spacer layer thickness is increased.

Large magnetic hyperfine fields acting on the Au nuclei, e.g. in Co/Au/CoO and related systems, result from the induced valence polarization of the Au atoms by the local *s*-*d* hybridization with the *d*-band of the nearest Co neighbors (Ref. [11], Ohnishi et al.). The degree of hybridization and thus the strength of the induced hyperfine field is thus strongly dependent on the Co-Au distance. Therefore we unfortunately cannot answer the question of whether EB is transferred through 'pinholes' or there exists a long-range mechanism through a non-magnetic spacer of many monolayers (ML) thickness. The issue of pinholes has been previously investigated and discussed for the case of Co/Au/CoO EB trilayers prepared in an identical way to the samples used in this work reference [7].

In contrast to LTNO, conventional macroscopic magnetic techniques, including SQUID magnetometry, vibrating sample magnetometry (VSM), Brillouin Light Scattering (BLS) and Ferromagnetic Resonance (FMR), are sensitive only to the magnetic layers [4] in the sample. The microscopic method of low energy muon spin rotation (LE-μSR) offers the possibility of investigating the induced conduction-electron spin polarization at many ML distance from a magnetic interface in a non-magnetic metal, because of the sensitivity of the implanted muons to very small magnetic fields [16]. However, those muons which are randomly stopped in the FM layers or near the ferromagnetic interface experience a wide distribution of large magnetic fields and do not contribute to the LE-μSR signal. Thus, excited-nuclear-probe techniques, such as LTNO, can complement these measurements by observing specifically the nuclear spin polarization (direction and magnetic hyperfine field strength) near the interface in multilayer systems (e.g. Co/Au/CoO) of both the magnetic (e.g. Co) and the non-magnetic (e.g. Au spacer) layers simultaneously.

Another microscopic experimental technique used to study induced magnetism is X-ray Magnetic Circular Dichroism (XMCD). However, the depth resolution of this technique, which uses the total electron yield detection method, is limited by the escape depth of the electrons, extending over several atomic layers. Furthermore, the signal from XMCD is sensitive to electrons with non-zero orbital angular momentum, i.e. *p*-, *d*- and *f*-electrons. The magnetic hyperfine field measured by LTNO in the Au spacers studied here is mainly due to spin polarization of *s*-electrons.

The present measurements were performed on Co/Au/CoO exchange bias and related systems with increasing Au layer thickness by means of LTNO. This type of EB system is characterized by extremely large exchange anisotropy. The magnetic Co layers consist of round or elliptical-shaped, predominantly (111)-oriented grains [17]. Due to their granular structure, there is basically one prominent direction, which is the direction of induced EB. Other prominent directions which might occur due to intrinsic anisotropies are averaged out. The dependence of the EB effect in Co/Au/CoO trilayers on the Au spacer thickness was previously studied via SQUID magnetometry [7]. A strong EB between the antiferromagnetic CoO and the ferromagnetic Co layers across thin Au spacer layers was observed even for a nominal Au thickness of 2.25 nm.

In this work, we report the first measurement of the EB effect in the Co ferromagnetic layer and at the same time in the adjacent Au non-magnetic spacer layer using the LTNO method. The magnetic properties of different Co/Au/CoO EB trilayers (and related systems) were studied. In order to understand the mechanisms leading to

EB, it is crucial to have information about the behavior of the magnetic moments at the AFM interface. This can be achieved by comparing the experimental findings obtained from Co/Au/CoO (EB) systems with those obtained from a Co/Au/Co system containing two FM/spacer interfaces and CoO/Au/CoO systems containing two AFM/spacer interfaces. Furthermore, we present the first demonstration of changes in magnetic orientation induced in the spacer layer in AFM/spacer/AFM trilayers as a function of the spacer thickness.

2 Experimental procedures

The [Co(16.4 nm)/Au(x nm)/CoO(2 nm)] trilayers were MBE-grown on hydrogen passivated Si(111) substrates with Au layer thicknesses of $x = 0.5, 0.75$ and 1.25 nm. For comparison, a [Co(16.4 nm)/Au(0.5 nm)/Co(16.4 nm)] trilayer with two FM Co/Au interfaces and two CoO(2 nm)/Au(x nm)/CoO(2 nm)] trilayers with two AFM CoO/Au interfaces were prepared, having Au layer thicknesses of $x = 0.5$ and 0.75 nm. The base pressure of the ultrahigh vacuum (UHV) chamber was 10^{-10} mbar and the samples were grown at room temperature. A 40 nm Ag capping layer was deposited on top of the trilayers to provide protection and a good thermal contact for the LTNO experiment. The method of CoO growth employed was that developed by Gruyters et al. [18] and has been used to achieve very large EB coupling energies in Co/CoO bilayers. First, a 2 nm layer of (111)Co is MBE grown and subsequently exposed in situ to pure oxygen at 10^{-5} mbar for 22 minutes. Previous Auger spectroscopic studies on as-prepared CoO layers reveal approximately a one-to-one ratio of Co and O [18]. X-ray diffraction confirmed that the Co metal layers had an fcc structure [7]. The EB samples were further characterized by SQUID magnetometry at 10 K after field cooling from $T = 300$ K (i.e. in the saturated state). They exhibited an exchange-bias field of 32, 27, and 19 mT for Au thicknesses of 0.5, 0.75, and 1.25 nm, respectively [7]. As an example, a SQUID curve of a H-Si(111)/Co/Au(0.5 nm)/CoO/Au layer is shown in Figure 1. The curve was recorded at 10 K after field cooling the sample in an external field of 400 mT.

All EB samples were then neutron activated for two to three days with thermal neutrons at a flux of 10^{13} n/cm^2/s in the BER-II research reactor at the Hahn-Meitner Institute, Berlin. The [CoO/Au(0.5 nm)/CoO] sample was activated for three days, while the [CoO/Au(0.75 nm)/CoO] sample was activated for 4 weeks. During this process, radioactive isotopes of ^{198}Au (2.7 d) and ^{60}Co (5.26 a) were produced from the naturally occurring stable Co and Au isotopes within the sample. No significant radiation damage is to be expected since fast neutrons were avoided at the irradiation site; careful X-ray examination of comparable samples irradiated under similar conditions for longer times showed a minimal increase in interface roughness. The samples were soldered together with a calibrated ^{54}MnAg nuclear thermometer onto a Ag holder using a Ga-2%Sn eutectic.

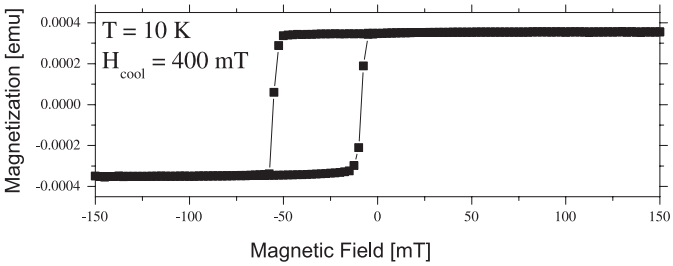

Fig. 1. SQUID hysteresis curve of a H-Si(111)/Co/Au(0.5 nm)/CoO/Au layer recorded at 10 K after field cooling in a field of 400 mT.

In order to induce the EB effect in the trilayers, an external field of > 400 mT was applied above room temperature. The samples were then top-loaded into a ^{3}He/^{4}He dilution refrigerator together with the ^{54}MnAg nuclear thermometer and cooled from the remanent state below the blocking temperature of about 200 K [17]. The induced EB effect is reduced because the samples are cooled in the remanent state and not in the saturated state [19]. At 4.2 K, a magnetic field was applied in the film plane and the samples were finally cooled to the base temperature of below 6 mK.

The distribution of the γ-rays following the β-decays of ^{198}Au and ^{60}Co and the electron capture decay of ^{54}Mn can be expressed as [10]:

$$W(\theta) = 1 + \sum_{k=2,4} B_k U_k A_k Q_k P_k(\cos\theta), \qquad (1)$$

where θ is the angle between the direction of the detector and the magnetic hyperfine field, and $B_k(T, B_{hf})$ are the nuclear orientation parameters, which are functions of both the temperature T and magnetic hyperfine field B_{hf}. U_k and A_k are known nuclear decay scheme parameters, Q_k are solid angle corrections for the finite detector size, and P_k are the Legendre polynomials. The γ-ray intensity angular distributions of the 412 keV, 1173 keV and 1332 keV, and 835 keV γ-rays from the decays of ^{198}Au, ^{60}Co, and the ^{54}Mn thermometer, respectively, were monitored with two Ge detectors: Detector D1 was mounted parallel to the plane of the trilayers and along the applied field direction, and detector D2 was also mounted parallel to the sample plane but perpendicular to D1 (see also the inset in Fig. 2). A typical energy spectrum of the EB samples, as measured by the Ge detectors, is given in Figure 2.

The γ-ray intensity depends on various factors, such as the amount of material, the neutron capture cross section and the radioactive half-life. In the present case, the thicknesses of the materials are 0.5 nm Au, 16.4 nm Co and 2 nm CoO. The neutron capture cross sections σ_c amount to 37 barn for ^{59}Co and 98.8 barn for ^{197}Au, and the half-life for the resulting radioactive isotope is 2.7 days (^{198}Au) and 5.26 years (^{60}Co). The measured γ-ray intensities are corrected for nuclear decay during the experiments. The black circle in the inset of Figure 2 represents an isotropic γ-ray distribution, which can be measured

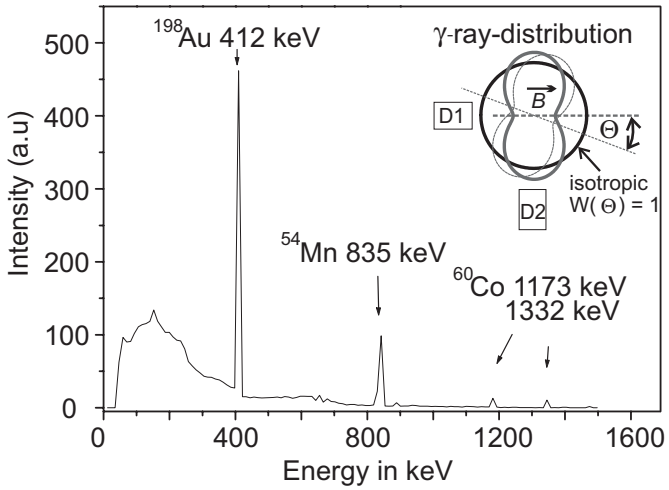

Fig. 2. Typical energy spectrum from a Co/Au/CoO sample containing the radioactive isotopes ^{60}Co and ^{198}Au together with the ^{54}MnAg thermometer. The experimental geometry and possible anisotropic γ-ray distributions are illustrated on the top right.

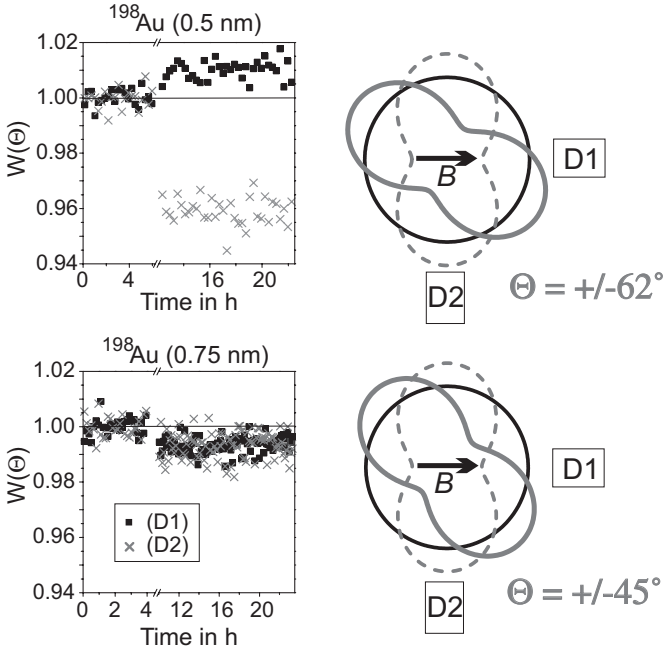

Fig. 3. *Left:* normalized γ-ray intensity from CoO(2 nm)/ Au(x)/CoO(2 nm), with $x = 0.5$ and 0.75 nm, determined by the detectors D1 (squares) and D2 (crosses); *Right:* Schematic of the γ-ray distribution, projected onto the sample plane, for the case of (i) an isotropic distribution (black solid line) and (ii) finite nuclear alignment ("Figure 8" pattern) parallel to the field (grey dashed line) and at an angle with respect to the field (grey solid line).

at higher temperatures, i.e. at 1 K, where the nuclei are not oriented ('warm counts': isotropic γ-ray distribution with $W(\Theta) = 1$). The values of the γ-ray intensities at 1 K were used to normalize the values obtained at very low temperatures ('cold counts': anisotropic γ-ray distribution), yielding the magnitude $W(\Theta)$ which is a function of different parameters as can be seen from equation (1):

$$W(\text{detector } i) = \frac{I_{cold}}{I_{warm}}. \quad (2)$$

The solid grey "figure-8" patterns represent the anisotropic ^{198}Au and ^{60}Co γ-ray distributions at low temperatures, indicating nuclear alignment. The orientation of the pattern indicates the in-plane direction of the nuclear alignment symmetry axis with respect to the applied field direction. The normalized γ-ray intensities can be studied then as a function of time during the cool-down procedure in the magnetically saturated state of the samples. From the cool-down curves, the average hyperfine field B_{hf} and the average angle Θ between the applied field axis and the nuclear magnetization of the specific radioactive probe isotope can be determined.

Furthermore, when the samples are in thermal equilibrium at mK temperatures, hysteresis curves can be obtained by plotting the normalized γ-ray intensities as a function of the applied magnetic field.

3 LTNO results for AFM/spacer/AFM systems

We began our investigation by first replacing the FM layer of a typical EB system with an AFM layer, in order to observe the dependence on spacer thickness of the induced magnetism in the Au spacer layer. Thus two CoO/Au(x)/CoO trilayers, with Au layer thicknesses of $x = 0.5$ and 0.75 nm, were prepared at the same time and under exactly the same conditions, to ensure that all preparation parameters were the same, except for the Au spacer thickness. Before top-loading the samples into the cryostat, a field of >400 mT was externally applied to it, to duplicate the procedure later employed for the EB systems. During the cooling down from 4 K to mK temperatures, a constant field of 500 mT was applied.

The cooling-down curves of the ^{198}Au γ-ray intensities are plotted in Figure 3 (left hand side) as a function of time for the two samples, down to a base temperature of about 6 mK. The corresponding cooling-down curves of the ^{60}Co γ-ray intensities are discussed later. The normalized γ-ray intensity at 1 K, $W(\Theta) = 1$, is marked by a horizontal line in each plot. The nuclear spin-lattice relaxation (NSLR) time for ^{198}Au can be estimated from the cool-down curve to be less than 30 minutes, consistent with the expected Korringa constant of $C_{\mathrm{K}} \cong 1$ sK. Firstly, both samples show a marked deviation from the isotropic γ-ray distribution (i.e. $W(\Theta) \neq 1$), indicating that on average the Au atoms in the spacer possess an induced magnetic moment and correspondingly exhibit magnetic alignment. Secondly, a drastic change in the Au nuclear spin alignment was observed as the Au spacer thickness was varied. For both samples, the γ-ray anisotropy measured by detector D2 (crosses) is $W(\Theta) < 1$, while the γ-ray anisotropy measured by D1 (squares) is $W(\Theta) > 1$ for the sample with Au(0.5 nm) and $W(\Theta) < 1$ for the

Table 1. *Average* angle Θ_{Au} of the nuclear alignment of the ^{198}Au moments in the Au spacer sandwiched between two AFM CoO layers with respect to the applied field axis. The average hyperfine field ("single-fraction model") and the hyperfine field calculated with the assumption that large Au polarizations are restricted to the CoO/Au interface ("two-fraction model") (see text), are given for two different Au spacer thicknesses, $x = 0.5$ nm and 0.75 nm.

Au-thickness x in nm	$\pm\Theta_{Au}$	"average" hyperfine field $\mid B_{HF} \mid$ [T] "one-fraction -model"	"interfacial" hyperfine field $\mid B_{HF} \mid$ [T] "two-fraction -model"
0.5	62(3)	23(2)	24(2)
0.75	45(2)	16(2)	21(2)

sample with Au(0.75 nm); this indicates a significant reorientation of the nuclear spin alignment induced in the Au layer.

On the right-hand side of Figure 3, a schematic representation of the shape of the γ-ray distribution is shown, projected onto the sample plane. This schematic neglects fourth-rank contributions to the angular distribution and assumes the ensemble of radioactive nuclei to be oriented along an axis at the angle $\pm\Theta$ to the applied field. It is shown for illustrative purposes. Furthermore, with the present setup, we cannot distinguish between positive and negative values of Θ. In order not to complicate the schematic diagram of the γ-ray distribution, the shape of the distribution $W(-\Theta)$ is not displayed. From the ratio of the normalized γ-ray intensities measured by the detectors D1 and D2, the in-plane average angles between the symmetry axis of the Au nuclear alignment and the applied field axis were determined; see Table 1. They are schematically shown in Figure 3. As seen in the table, the average in-plane angle for the sample with [Au(0.5 nm)] was found to be $\pm 62(3)^\circ$ at 500 mT. In contrast, for the sample with [Au(0.75 nm)], the nuclear spin orientation of the Au moments was observed to rotate to an in-plane angle of $\pm 45(2)^\circ$.

There are two possibilities to determine the hyperfine field of ^{198}Au in a non-magnetic Au spacer from the measured intensities: the first follows the assumption that all nuclei in the Au spacer experience the *same* average hyperfine field ("single-fraction model"). In the second approach, the assumption is made that only the Au nuclei situated at an interface with Co or CoO are subject to a large hyperfine field. The Au spacer atoms further away from the interfaces are assumed to experience negligible hyperfine fields in this "two-fraction model". As stated in the introduction, LNTO is not sensitive to hyperfine fields $\leq 3\ T$. The calculation of this latter model is carried out by introducing a fraction f into equation (1):

$$W(\theta) = 1 + f \times \sum_{k=2,4} B_k U_k A_k Q_k P_k(\cos\theta), \qquad (3)$$

where $1 - f$ is the fraction of ^{198}Au nuclei experiencing a negligible hyperfine field. The second approach was experimentally confirmed for FM/spacer interfaces by [13], who performed Perturbed Angular Correlation (PAC) experiments on a Fe/Ag interface and by [14] using Mössbauer spectroscopy on Ni/Au and Fe/Au multilayers as well as by [12] applying LTNO to Fe/Ag multilayers. It was found in these experiments that only the Au or Ag nuclei immediately adjacent to the ferromagnetic material experience large hyperfine fields, as described above.

The average Au hyperfine field given in Table 1 (middle column) was calculated from the measured γ-ray intensities using equation (1) and assuming a temperature as given by the ^{54}MnAg thermometer in thermal contact with the cold finger.

Using this "single-fraction model", a large reduction of the average hyperfine field $\mid B_{hf} \mid$ from 23(2) T to 16(2) T was found as the Au spacer thickness increased from 0.5 nm to 0.75 nm. This can also be expressed as a reduction in the degree of nuclear spin alignment by a factor of $\frac{B_2[\text{Au}(0.75\text{ nm})]}{B_2[\text{Au}(0.5\text{ nm})]} = 0.54$.

Now assuming instead that only Au sites directly adjacent to the CoO interface experience a nonzero hyperfine field, i.e. applying the "two-fraction model", the average Au hyperfine fields for these sites were recalculated for both samples. The resulting values (24(2) T [Au(0.5 nm)] and 21(2) T [Au(0.75 nm)]) are shown in the right column of Table 1. A comparison of the results for the hyperfine fields $\mid B_{hf} \mid$ strongly supports the "two-fraction model", since the hyperfine field values at the CoO/Au interfaces are – within error bars – equal for the two samples, while the *average* hyperfine field (i.e. the "single-fraction model") decreases with increasing Au spacer thickness. Thus, large polarizations of the nuclear Au moments are restricted to the interface layers. It should be mentioned that a thickness of 0.5 nm Au would correspond to roughly two monolayers of Au.

We now turn to the corresponding cooling-down curves of the ^{60}Co γ-ray intensities for the two CoO/Au(x)/CoO samples. For both samples *no* γ-ray anisotropy – within error bars – from the ^{60}Co (in CoO) was observed at low temperatures ($W(\Theta) \simeq 1$). As an example the ^{60}Co cooling-down curve is shown in Figure 4b for the CoO/Au(0.5 nm)/CoO sample together with the corresponding ^{198}Au coolingdown curve. Given an experimentally determined magnetic hyperfine field of +49.5 T for ^{60}Co in CoO, as measured by Okada [20] using NMR (for calculations of B_{HF} see also [21]), the expected ^{60}Co γ-ray anisotropy would amount to $W(0^\circ) = 0.09$, assuming full magnetic alignment at a measurement temperature of $T = 5.7$ mK. This is an order of magnitude less than the measured value.

A possible explanation for the negligibly small nuclear alignment of ^{60}Co (in CoO) at these temperatures is a very long ^{60}Co nuclear-spin lattice relaxation (NSLR) time in CoO, so that the nuclei cannot be cooled to the lattice temperature during the duration of the experiment. The NSLR times of ^{60}Co in bulk CoO are in fact expected to be of the order of weeks for the following

reasons: (i) phonons cannot make a significant contribution to the relaxation, since they are hardly excited at these temperatures and are only weakly coupled to the nuclear moments;(ii) magnons, owing to the large energy gap, are not excited at these temperatures. For example, for non S-state ions, the magnon energy gap E_g is comparable to kT_N [22]. Considering that a NSLR time of 38 days at temperatures below 60 mK [23] has been reported for $MnCl_2.4H_2O$, which has an energy gap of $E_g/k \sim 1$ K, then the NSLR time of ^{60}Co in bulk CoO, with $T_N \cong 300$ K, should be even much longer.

Another possible explanation for the observed near-zero ^{60}Co γ-ray anisotropy is that on average, the CoO grains are not magnetically aligned. However, this would appear unlikely. Given that the Au has achieved some alignment at the interface, as observed, this implies that the Co ions on the CoO side of the same interface are also at least partially aligned, since the exchange coupling with them is responsible for the induced moments on the Au atoms. It should be noted that the ^{60}Co (in CoO) signal is not exclusively due to the CoO/Au interface, but is an average over the whole CoO layer (its thickness of 2 nm corresponds to about 8 ML). The partial alignment at the CoO interface may be attributed to the existence of uncompensated moments in the CoO interface layers, as were experimentally found by Gruyters et al. [17]. For further discussion of these results see Section 6.

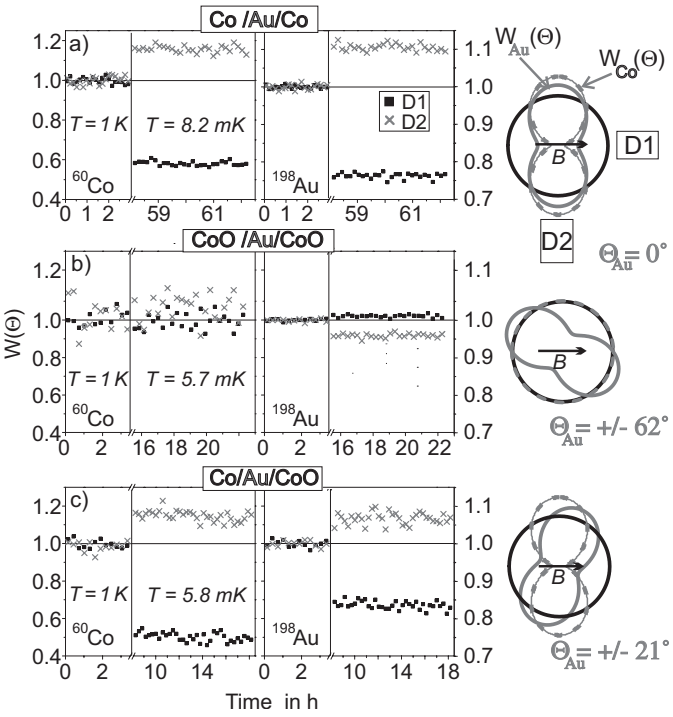

Fig. 4. Normalized γ-ray intensities for three different magnetic systems: Co/Au/Co (a); CoO/Au/CoO (b); Co/Au/CoO (EB) (c), each with a 0.5 nm Au spacer, during the cooling-down process in an applied field of 500 mT. The experimental geometry and the γ-ray distributions are illustrated on the right.

4 LTNO results for EB FM/spacer/AFM and related systems

In order to understand the different magnetic interactions induced in the Au spacer at the interfaces in EB systems, we have investigated all three combinations; FM/spacer/FM, AFM/spacer/AFM and the FM/spacer/AFM EB system. The normalized γ-ray intensities emitted from the ^{60}Co and ^{198}Au nuclear probes during the cooling down were monitored by the detectors D1 (square symbols) and D2 (cross symbols) and are plotted in Figure 4 as a function of time for the three different magnetic systems: a) Co/Au/Co; b) CoO/Au/CoO; and c) Co/Au/CoO [= EB system]. The Au spacer thickness was kept constant at 0.5 nm, which is approximately 2 ML of Au. These measurements were carried out in an applied field of 0.5 T, at which the FM Co layer is magnetically saturated.

The isotropic value of the normalized γ-ray intensity at 1 K, $W(\Theta) = 1$, is marked by a flat horizontal line in each plot. For consistency we have repeated the ^{198}Au cooling-down curve (Fig. 4b) originally shown in Figure 3a for the CoO/Au(0.5 nm)/CoO sample. Similar to Figure 3, on the right hand side of Figure 4, a schematic diagram of the shape of the γ-ray distribution, projected onto the sample plane, is given for both isotopes, using the same simplifications described for Figure 3.

At temperatures far below 1 K, the γ-ray distribution of ^{60}Co in the Co/Au/Co trilayer and in the Co/Au/CoO EB-system was observed to be anisotropic, and as expected, aligned along the external applied magnetic field (see Figs. 4a and c). In contrast, as discussed above, no ^{60}Co γ-ray anisotropy was observed for the CoO/Au/CoO system (see Fig. 4b). In comparison to ^{60}Co, the ^{198}Au γ-ray distribution shows a different behavior. For the two samples containing CoO layers (see Figs. 4b and c), the nuclear alignment axis determined from the ^{198}Au γ-ray intensities (detectors D1, D2) was found to be canted (non-collinear) with respect to the applied field.

In particular, in comparison to the two other systems, the canting of the nuclear ^{198}Au moments in the CoO/Au/CoO samples was large enough to reverse the sense of the intensity deviation of the γ-radiation at mK temperatures, monitored by the two detectors, with respect to the "warm" intensity at 1 K: an intensity increase (decrease) was observed by D1 (D2); see Figure 4b. In contrast, no canting of the induced magnetic Au moments was observed for the Co/Au/Co sample (see Fig. 4a). A summary of this situation is schematically illustrated in Figure 4 (right). From the values of the γ-ray anisotropy, $W(\Theta)$, as measured by both detectors, the angle between the alignment axis and the external applied field as well as the average hyperfine fields were determined using equation (1) and equation (3), see Table 2.

In summary, two basic trends have been observed when replacing the Co interfaces with CoO interfaces. They are shown in Table 2: (i) the average angle Θ between the direction of the magnetic hyperfine field and the applied saturating field increases from 0° to 62°; while (ii) the

Table 2. *Average* angle Θ_{Au} of the axis of nuclear alignment of the Au moments relative to the applied field axis in a 0.5 nm Au spacer sandwiched between two magnetic layers, and the average Au hyperfine field $\mid B_{HF} \mid$ [T] for three different magnetic sample types: FM/Au/FM, FM/Au/AFM, and AFM/Au/AFM, with FM = Co and AFM = CoO.

Au(0.5 nm) in	$\pm\Theta_{\mathrm{Au}}$	Average hyperfine field $\mid B_{HF} \mid$ [T]
Co/Au/Co	0	78(3)
CoO/Au/CoO	62(3)	23(2)
Co/Au/CoO	21(4)	48(4)

average hyperfine field acting on the ^{198}Au nuclei decreases. It is interesting to note that the average hyperfine field of Au in Co/Au/Co is 78(3) T, which is surprisingly close to the measured value of 87.02(11) T known for Au as an impurity in fcc Co [24]. Unfortunately, more precise knowledge of the structure of the Co/Au interface, or whether Au has diffused into the Co layer, cannot be obtained from the level of resolution observable by LTNO.

However, appreciable diffusion of single Au impurities into Co and CoO can be neglected for various reasons: Firstly, Co and Au are immiscible in the bulk [25]. Secondly, investigations on Co/Au film-substrate systems show that only at elevated temperatures do Au atoms either segregate to the surface [26] or occupy interstices between Co clusters [25]. Because all our experiments were performed close to room temperature or below it, segregation plays no role for our CoO/Au/Co system, as is also evidenced by the detailed analysis of the Auger electron spectroscopy data presented in reference [7]. That is, the value of the Au hyperfine field given above originates from Au at Au/Co interfaces rather than from single Au impurities in Co.

To derive the average hyperfine field, the temperature first must be determined. Where possible, the temperature of the layer systems investigated was measured directly from the ^{60}Co γ-ray intensity emitted from the sample, provided it contained a FM Co layer. It should be noted that the ^{60}Co signal for the Co/Au/CoO EB system is composed of two fractions: (i) ^{60}Co in (16.4 nm Co); (ii) ^{60}Co in (2 nm CoO). This has been accounted for by using a two-fraction model as described above (see Eq. (3)) and assuming the ^{60}Co (in CoO) γ-ray contribution to be isotropic. The latter assumption is justified by the results described in Section 3.

Since the hyperfine field of ^{60}Co in Co, $B_{HF} = -21.63$ T [27] is well known, and the FM Co layer is magnetically saturated, the ^{60}Co γ-ray anisotropy yields the correct sample temperature. For example, as given in Figure 4a, the base temperature of the Co/Au/Co sample was 8.2(5) mK, while it was 5.8(5) mK during the experiment with the Co/Au/CoO EB trilayer (Fig. 4c). The small difference of ~ 2 mK could be due to differing amounts of radioactive heating due to the β-decay for the ^{60}Co (a typical sample of 2 μCurie produces ~ 1.2 nW of thermal heating).

As a final comment concerning the values reproduced in Tables 1 and 2, the ratio $(W(D1)-1)/(W(D2)-1)$ of the normalized γ-ray intensities measured by the two detectors is independent of the temperature and magnitude of the hyperfine field, when 4th order terms can be neglected, as in the case of ^{198}Au. From this ratio, reasonable out-of-plane deviations can be restricted to $\pm 20°$. The resulting in-plane projected angles and magnetic hyperfine fields are largely insensitive to these possible out-of-plane angles. The error bars in Tables 1 and 2 reflect both the statistical and potential systematic errors (including external dipolar fields) resulting from the above considerations. The sign of the magnetic hyperfine fields are unknown since γ-decay conserves parity and cannot be used to determine the sense in which the spins are directed along a particular axis without an additional circular polarization measurement.

5 LTNO measurement of the EB effect

Finally, in order to observe the induced EB effect with LTNO, hysteresis measurements were performed, detecting the γ-radiation emitted by the radioactive probes ^{60}Co and ^{198}Au from Co/Au/CoO samples as a function of the applied field in a direction parallel to the external field (D1) and in-plane but perpendicular to it (D2). As an example, the result for the EB system with a 0.5 nm Au spacer is shown in Figure 5. Since the sample was previously cooled from the remanent magnetization state, it is in the EB state when the cryostat reaches its base temperature of about 6 mK. The hysteresis curve was started at +500 mT, i.e. with the applied field parallel to the initial magnetizing field.

Figure 5 shows the normalized γ-ray intensities monitored by both detectors (D1, D2) for ^{198}Au (left) and ^{60}Co (middle), emitted from the Co/Au(0.5 nm)/CoO trilayer as a function of the applied field. Additionally, the ^{54}MnAg γ-ray intensities (right) are plotted for comparison. The measured γ-ray intensities for all three isotopes show a significant deviation from W(Θ)=1 at low (mK) temperatures, indicating nuclear alignment. As a function of the applied field, the γ-ray intensity of the ^{54}MnAg thermometer shows a completely symmetric curve for positive and negative fields (Fig. 5 right). Furthermore, there was no difference between the γ-ray intensities measured with increasing and decreasing applied magnetic fields for the ^{54}MnAg nuclear thermometer, which represents essentially a paramagnetic spin system. In contrast, for both the ^{60}Co and the ^{198}Au γ-ray intensities, two maxima (D2: minima) are observed at lower magnetic fields, – i.e. when the magnetization reversals take place –, one on each side of the zero field axis but not symmetric with respect to $B = 0$. This striking asymmetry in the position (with respect to the zero field axis) and also in the height of the observed maxima (D1) and minima (D2) can thus not be due to temperature effects (which would also appear in the thermometer data), and must instead be attributed to the EB effect.

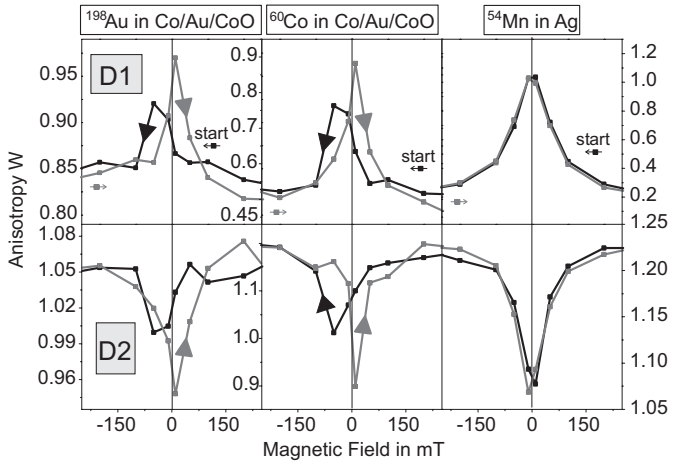

Fig. 5. Hysteresis measurement: normalized γ-ray intensity of ^{60}Co and ^{198}Au in the EB state, and of the ^{54}MnAg thermometer as a function of the applied field for detector D1 (top) and detector D2 (bottom).

Comparing the curves obtained for the ^{60}Co and ^{198}Au γ-ray intensities, it is obvious that the Au nuclear moments at the Au/Co interface are strongly polarized by the neighboring Co atoms. The Au nuclear magnetization appears to follow the Co ferromagnetic magnetization during the magnetization reversal process, leading to the same qualitative dependence of the γ-ray intensity on the external field. The only differences are the absolute values of the normalized γ-ray intensities and a canting angle between the alignment axis of the Au and the Co nuclei, which was discussed above for the case of magnetic saturation.

The positions of the two maxima are not symmetric with respect to the zero field axis, but are shifted towards negative fields. This can be expected for an EB system previously cooled in a positive cooling field. Taking the strength of the EB to be the shift in the center of the interval between the two maxima along the magnetic field axis, the measured EB field is found to be 20 mT for a Au thickness of 0.5 nm. Considering the fact that the samples were cooled from their remanent state, this EB field is consistent with that measured by SQUID magnetometry at 10 K [17] on similar samples.

Monitoring the counting rates in the two γ-ray detectors, D1 and D2, the measurements may also be used to distinguish between magnetic reversal processes dominated by domain wall motion and those dominated by domain rotation. Referring to the two peaks, the data indicate a height asymmetry of the γ-ray intensities as the magnetic field is varied along the hysteresis curve (see Fig. 5) for both the ^{60}Co and ^{198}Au radioactive probes, but (as expected), not for the ^{54}MnAg thermometer. This height asymmetry can presumably be attributed to different magnetization reversal processes on the decreasing and increasing field branches. The flatter response across the magnetization reversal (left-hand peak structures for Co and Au probes in Fig. 5) can be interpreted as being dominated by a breakup into domains with parallel or antiparallel orientation with respect to the applied field and showing less spin rotation. The higher ratio on the return sweep (right-hand peak structures in Fig. 5) is consistent with a magnetization reversal process that is dominated by domain rotation. It should be noted that no peak would be observed in the simple case where the sample contains only domains oriented parallel or antiparallel to the applied field. These features are consistent with the asymmetric reversal processes on opposite sides of the same hysteresis loop observed for an as-prepared Co/CoO multilayer system using polarized neutron reflectometry (see Ref. [28]).

6 Discussion

We have studied the Au nuclear spin polarization in CoO/Au/CoO trilayers as a function of the Au spacer thickness using LTNO. For the case of AFM CoO/Au interfaces, we have observed that large magnetic spin perturbations on the Au atoms were restricted to those atoms in direct contact with the antiferromagnetic CoO surface, similar to many other theoretical and experimental studies on FM/noble-metal interfaces (see e.g. Refs. [11–14]). This indicates that the technique of LTNO is sensitive only to those non-magnetic radioactive probes located directly at the interfaces with a FM or an AFM surface. This means that the important question of whether EB can be transferred through many atomic layers of a non-magnetic spacer, or only via direct contact through "pinholes", cannot be tested using this technique.

In addition, it was observed that CoO causes a canting in the induced Au magnetic moments with respect to an external applied magnetic field. Furthermore, this canting appears to be dependent on the spacer thickness in CoO/Au/CoO trilayers, indicating an interaction between the two CoO magnetic layers. For these samples the canting cannot be due to a structural magnetic anisotropy, since STM measurements have shown that the CoO grains are almost round and have no intrinsic preferred orientation [17]. In this case, the induced magnetic EB anisotropy in the CoO/Co is the only prominent magnetic axis and is determined by the direction of an external applied field. As a possible explanation for the observed canting, it was found previously that the spin-axis distribution energetically favors those spin axes most nearly perpendicular to the cooling field direction for thin films of CoO grown on MgO [29].

The near zero ^{60}Co γ-ray anisotropy observed in the CoO/Au/CoO trilayer systems has been attributed to very long NSLR times for Co in CoO at low temperatures, cf. Section 3. Thus, unfortunately, we could not directly demonstrate the alignment of the Co moments within the CoO layers. However, the observation of a Au γ-ray anisotropy at the interface implies a partial alignment of the CoO surface layer and it is attributed to the existence of uncompensated moments in the CoO interface layers. Uncompensated Co spins were first observed in CoO films grown on SiO_2, leading to a remanent magnetization in field-cooled samples [30]. Hysteresis measurements

performed on our CoO/Au/CoO samples up to 1 T showed no changes in the canting angle within the error limits [31]. Thus the uncompensated Co spins possess a relatively large magnetic anisotropy compared to this external field.

Having experimentally established that the induced moments of Au in a CoO/Au/CoO trilayer are canted, we compared the effects of replacing the CoO layers one by one with Co layers. Table 2 compares the induced Au hyperfine fields (angle and magnitude) for all three trilayer combinations. The average canting angle was found to be significantly reduced by replacing one CoO layer by a Co layer (Co/Au/CoO EB system), while for the Co/Au/Co system, i.e. on replacing both CoO layers by Co, the Au moments are aligned parallel to the external field (no canting angle), as expected. Moreover, this effect would appear to be not simply additive: i.e., in the EB system the induced Au moments are aligned more closely to the external field than would be expected from a simple superposition of the two interfaces. Therefore, the effect of replacing one CoO layer by Co is to pull the induced moments of the Au layer adjacent to the remaining CoO layer towards the alignment axis of the external field. Finally, in previous studies on an "as prepared" EB Co/CoO system without a Au spacer, it was estimated that at least one ML of a 20 Å CoO film is uncompensated and is aligned along the induced EB anisotropy direction [17].

Comparing to other systems, it has been observed previously by Ohldag et al. [32] that the uncompensated spins at the interface in an Fe/NiO EB system are collinear. Following the model for EB in granular FM/AFM systems proposed by Stiles and McMichael [33], the uncompensated moments act as possible centers for the nucleation of domain walls in the AFM layer. This model does not necessarily imply collinear alignment of the moments at a FM/AFM interface.

However, when considering a non-magnetic spacer, the situation might change, as we observed for our Co/Au/CoO trilayers, where it was found that the effect of adding a Au spacer between Co and CoO is to allow the interfacial Co moments in CoO (which are in direct *s-d* hybridization with the interfacial Au atoms) to relax into a canted magnetic structure at the interface, thus reducing the net moment of the uncompensated spins in the direction of the induced EB anisotropy. This might be one of the mechanisms leading to the observed strong decrease in the EB effect with increasing spacer thickness [7].

7 Conclusions

The EB effect was observed for the first time in the interfacial Au atoms of a non-magnetic spacer layer sandwiched between FM Co and AFM CoO. The induced Au magnetic moments seem to simply follow the FM Co moments during the magnetization reversal processes. LTNO has been shown to be sensitive only to the Au atoms in direct contact with magnetic surface atoms, making this technique valuable for understanding the interactions at the interface. We are the first to observe this local sensitivity for the case of an AFM/non-magnetic spacer interface using LTNO.

Furthermore, we found a non-collinear alignment of the Au nuclear moments with respect to the applied field for the Co/Au/CoO EB system and the related CoO/Au/CoO trilayers. From a comparison of the induced Au magnetic moments in different trilayer systems – FM/spacer/AFM (EB-system), FM/spacer/FM and AFM/spacer/AFM – the canting of the Au magnetic moments was found to originate at the CoO/Au interface. Moreover, measurements on CoO/Au/CoO trilayers showed that this canting depends on the spacer thickness. This non-collinear alignment of the magnetic moments at an AFM/non-magnetic interface should be considered for theoretical models of EB which include a non-magnetic spacer layer.

A detailed explanation of the microscopic mechanism of EB is yet to be formulated [4]. The situation becomes even more complicated when a spacer is added between the FM and AFM layers. We believe that the application of a novel excited-nuclear-probe technique, such as LTNO, sheds new insight that other techniques cannot achieve. Finally, systematic experimental results on a particular system will hopefully stimulate detailed calculations to explain this phenomenon.

We thank the staff of BER II for assistance with the neutron irradiation. One of us (MJP) thanks the Humboldt Foundation and the DFG for support during the course of this work.

References

1. P. Grünberg, R. Schreiber, Y. Pang, M.B. Brodsky, H. Sowers, Phys. Rev. Lett. **57**, 2442 (1986)
2. N.J. Gökemeijer, T. Ambrose, C.L. Chien, Phys. Rev. Lett. **79**, 4270 (1997)
3. W.H. Meiklejohn, C.P. Bean, Phys. Rev. **102**, 1413 (1956)
4. J. Nogués, I.K. Schuller, J. Magn. Magn. Mater. **192**, 203 (1999)
5. T. Mewes, B.F.P. Roos, S.O. Demokritov, B. Hillebrands, J. Appl. Phys. **87**, 5064 (2000)
6. L. Thomas, A.J. Kellock, S.S.P. Parkin, J. Appl. Phys. **87**, 5061 (2000)
7. M. Gruyters, M. Gierlings, D. Riegel, Phys. Rev. B **64**, 132401 (2001)
8. M. Nývlt, T. Katayama, Y. Suzuki, S. Yuasa, J. Franta, Š. Višňovsky, *16th ICMFS, Natal*, edited by M.N. Baibich, A.B. Antunes (Instituto de Física UFRGS, 2000), p. 216
9. K. Inagawa, K. Kamigaki, S. Miura, J. Phys. Soc. Jpn **31**, 1276 (1971)
10. N.J. Stone, H. Postma, *Low Temperature Nuclear Orientation* (Elsevier Science, 1986)
11. S. Ohnishi, M. Weinert, A.J. Freeman, Phys. Rev. B **30**, 36 (1984)
12. T. Phalet, M.J. Prandolini, W.D. Brewer, P. De Moor, P. Schuurmans, N. Severijns, B.G. Turrell, A. Van Geert, B. Vereecke, S. Versyck, Phys. Rev. Lett. **86**, 902 (2001)
13. B.-U. Runge, M. Dippel, G. Filleböck, K. Jacobs, U. Kohl, G. Schatz, Phys. Rev. Lett. **79**, 3054 (1997).

14. Y. Kobayashi, S. Nasu, T. Emoto, T. Shinjo, Hyp. Int. **94**, 2273 (1994)
15. F. Wilhelm, P. Poulopoulos, G. Ceballos, H. Wende, K. Baberschke, P. Srivastava, D. Benea, H. Ebert, M. Angelakeris, N.K. Flevaris, D. Niarchos, A. Rogalev, N.B. Brookes, Phys. Rev. Lett. **85**, 413 (2000)
16. H. Luetkens, J. Korecki, E. Morenzoni, T. Prokscha, M. Birke, H. Glückler, R. Khasanov, H.-H. Klauss, T. Ślezak, A. Suter, E.M. Forgan, Ch. Niedermayer, F.J. Litterst, Phys. Rev. Lett. **91**, 017204 (2003)
17. M. Gruyters, D. Riegel, Phys. Rev. B **63**, 052401 (2001)
18. M. Gruyters, D. Riegel, J. Appl. Phys. **88,** 6610 (2000)
19. P. Miltényi, M. Gierlings, M. Bamming, U. May, G. Güntherodt, J. Nogués, M. Gruyters, C. Leighton, I.K. Schuller, Appl. Phys. Lett. **75**, 2304 (1999)
20. K. Okada, H. Yasuoka, J. Phys. Soc. Jpn **43**, 34 (1977)
21. K. Motizuki, J. Phys. Soc. Jpn **15**, 888 (1960)
22. V. Jaccarino, *Magnetism 2A*, edited by G.T. Rado, H. Suhl, (Academic Press, New York, 1965)
23. M. Le Gros, A. Kotlicki, B.G. Turrell, Hyp. Int. **77**, 203 (1993)
24. K.-H. Ebeling, R. Eder, E. Hagn, E. Zech, M. Deicher, Z. Naturforsch. a **41**, 95 (1986)
25. N. Marsot, R. Belkhou, F. Scheurer, B. Bartenlian, N. Barrett, M.A. Delaunay, C. Guillot, Surf. Sci. **377-379**, 225 (1997)
26. M. Speckmann, H.P. Oepen, H. Ibach, Phys. Rev. Lett. **75**, 2035 (1995)
27. E. Zech, E. Hagn, H. Ernst, G. Eska, Hyp. Int. **4**, 342 (1978)
28. M. Gierlings, M.J. Prandolini, H. Fritzsche, M. Gruyters, D. Riegel, Phys. Rev. B **65**, 092407 (2002)
29. J.H. Greiner, A.E. Berkowitz, J.E. Weidenborner, J. Appl. Phys. **37**, 2149 (1966)
30. T. Ambrose, C.L. Chien, Phys. Rev. Lett. **76**, 1743 (1996)
31. M. Gierlings, Ph.D. Dissertation, Freie Universität Berlin, (2002)
32. H. Ohldag, T.J. Regan, J. Stöhr, A. Scholl, F. Nolting, J. Lüning, C. Stamm, S. Anders, R.L. White, Phys. Rev. Lett. **87**, 247201 (2001)
33. M.D. Stiles, R.D. McMichael, Phys. Rev. B **59**, 3722 (1999)